Fuel Economy of Hybrid Electric Flight

Link sito dell'editore: https://www.sciencedirect.com/science/article/abs/pii/S0306261917312631

Link codice DOI: https://doi.org/10.1016/j.apenergy.2017.08.229

Citazione bibliografica dell'articolo: Teresa Donateo, Luigi Spedicato, "Fuel economy of hybrid electric flight", Applied Energy, 2017, Volume 206, Pages 723-738

Fuel Economy of Hybrid Electric Flight

Teresa Donateo, Luigi Spedicato
Department of Engineering for Innovation
University of Salento, Italy

Abstract

The present investigation addresses the problem of evaluating the endurance of hybrid electric aircraft and discusses the effect of battery specifications and the engine working points on fuel economy. In particular, the endurance per unit mass of fuel of a hybrid power system is calculated by assuming a constant power-level flight performed with alternate cycles of battery charging and discharging (ON-OFF strategy). The computation of the fuel economy requires accurate models for the time, the power and the energy associated with battery charging and discharge processes. In order to reach this goal, two approaches proposed in literature to evaluate electric endurance were discussed, amended and validated through comparison with experimental data. A model for constant-current/constant voltage battery charge was also presented and validated with literature experimental data. In order to explain how these models can be applied to real applications, a parallel hybrid power system was sized and analyzed for a medium-altitude long-endurance unmanned aerial vehicle. Lithium polymer batteries and two stroke diesel engines were considered and three different hybridization degrees were analyzed. The results showed a trade-off between electric flight time and overall endurance per unit mass of fuel and an improvement up to 12% in fuel consumption with respect to a non-hybrid case with the same engine.

Corresponding author

Prof. Teresa Donateo
Department of Engineering for Innovation
Università del Salento, Lecce, Italy
Via per Arnesano, 73100 Lecce
Phone number: +39 0832 297 754
e-mail: teresa.donateo@unisalento.it

1 Introduction

In conventional aircraft powertrains with thermal engines, the amount of energy stored on board is not a limiting factor because of the very high gravimetric and volumetric densities of liquid fuel [1]. For these systems, endurance is usually evaluated in conditions of level flight using the well-known Breguet formulas [2]. Breguet formulas cannot be applied to battery powered aircraft because of the complex behavior of electric storage systems that makes arduous to establish the actual energy available during the flight and the overall efficiency of electric flight.

Even if some formulas for electric steady rectilinear level flight were proposed in literature [3,4], the problem is not trivial because of the dependence of battery capacity on several parameters including current drawn, temperature, aging and cycling. Another problem is the lack of useful experimental data since batteries are usually tested at constant current (see for example [5] and [6]). For this reason, Traub [7] and Avanzini et al. [8] performed specific constant power discharge tests that attempted to reproduce the power request in a steady level flight. However, the approaches of these authors do not take into account the technological limits to the power drawn from the battery, and in particular its maximum continuous current that also affects the energy density.

To evaluate electric endurance, *EE*, Donateo et al. [9] proposed a mission-based approach that can take into account the variability of power request for both propulsion and auxiliaries (payload, avionic, etc.). A similar approach is also used by Fuller [10]. During the preliminary design of an electric or hybrid electric power system, however, it could be more useful to have a simple formula for endurance than a detailed simulation tool.

In this work, amendments to the approaches of [3] and [11] are suggested to improve their accuracy and to put into evidence the effect of battery specification. Moreover, the proposed formulations for battery discharging time are expressed in terms of datasheet specifications to make easier the application to real cases. Their accuracy is experimentally validated over a wide range of batteries versions and discharging conditions.

As for the time and the energy required for charging the batteries, the authors couldn't find an appropriate model but some experimental data are reported in [12]. Therefore, another original contribution of the paper is the development and the validation of a model to estimate the time, the energy and the power required to charge a battery according to the selected charging current. Such a model is essential in the study of a hybrid electric airplane where batteries can be recharged in flight when excess propulsive power is available (for example in cruise or during the plane's descent).
All in all, fuel economy in a hybrid electric aircraft cannot be calculated with a universally valid equation because it depends on the architecture (series or parallel), the hybridization degree (electric power to total power), the engine design and the energy management strategy of the power system[13]. This work describes a methodology to evaluate the endurance of a hybrid power system that assumes a constant power - level flight performed either in thermal mode or swapping between battery charging and electric flight (ON-OFF strategy). The investigation is also innovative in comparing a conventional powertrain and three hybrid power systems for the same aircraft with different hybridization degrees.
The paper is organized as follows. It starts with a short review of the state of the art of engines, motors and batteries for aircraft with particular reference to unmanned aerial vehicles. Then, battery charging and discharging models are described (Section 3) together with their amendments and experimental validation. These models are used in Section 4 to formulate the endurance per unit mass of fuel of a hybrid electric power system with the proposed ON-OFF strategy. As an example of how the proposed approach can be used for real applications, the sizing and the analysis of a parallel hybrid electric aircraft is performed in Section 5. The results of the proposed test case are presented in Section 6 where the effects of battery specification and engine working points on fuel economy are discussed.

2 Components of a hybrid electric aircraft

The main components of a parallel hybrid electric powertrain and the corresponding power flows are shown in Figure 1. For the scope of this study, the propeller and the gearbox can be modeled with a constant global propulsive efficiency η_P defined as the ratio between the thrust horse power (THP) required to move the aircraft (at the selected speed and altitude) and the brake horse power (BHP) to be generated by the power system.

The THP is the product of thrust and true air speed and can be calculated as [2]:

$$THP = \frac{1}{2}\rho U^{3} S \cdot C_{D0} + \frac{2W^{2}K}{\rho US} \quad (1)$$

Where W is the aircraft weight, U is the true air speed, ρ is the atmospheric air density at the selected flight altitude, S is the wing area, C_{D0} and K are aerodynamic coefficients of the aircraft (namely the zero lift drag and the induced drag factor, respectively).

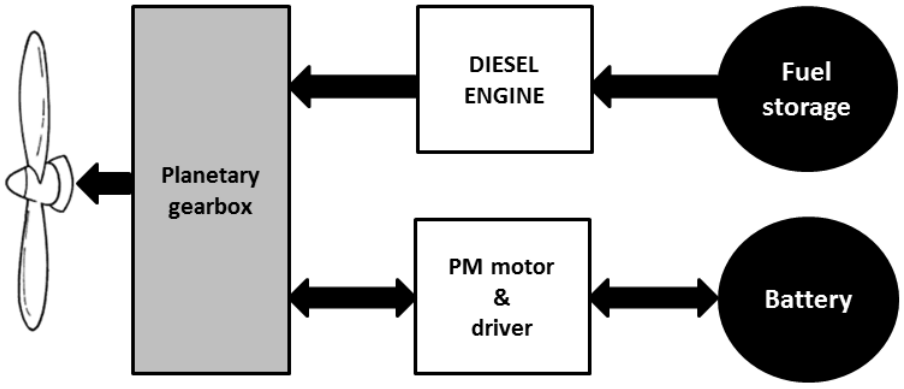

Figure 1 – A parallel hybrid power systems

2.1 The engine

Even if the proposed approach can be extended to other applications, this work focuses on Unmanned Aerial Vehicles (UAVs) where the possibility to fly in electric mode for a certain

amount of time is a specific requirement of the hybrid electric powertrain in order to reduce the thermal and acoustic signature [14,15].

In the case of UAVs, electric propulsion is preferred when BHP does not exceed few kilowatts. For higher BHPs the types of engines reported in Table 1 [16] are used.

Table 1 - Engines for UAVs [16]

UAV Type	Engine type	Power range (kW)
Mini	Two-stroke gasoline	1-15
Small tactical	Rotary engine (Wankel)	15-70
MALE (Medium Altitude Long Endurance)	Four stroke piston engines	60-190
MALE (Medium Altitude Long Endurance)	Turbo-prop	190-370
HALE (High Altitude Long Endurance)	Turbo-Jet/Fan	>370

Studies in literature show that, at current technology levels, the development of a hybrid-electric aircraft in the rage of power higher than 200kW appears challenging. Improved aerodynamics, reduced structural mass and more advanced batteries are necessary to achieve even a modest range capability [17].

Rotary Wankel engines have the advantage of a very high power per unit mass but are also characterized by very poor fuel economy. Piston engines are the most interesting for hybrid applications and almost the only type of engine used in the hybrid prototypes that have been so far built and tested [18-20]. Among piston engines, Diesel machines are becoming more and more interesting for their higher efficiency and for the possibility to burn either diesel fuel or kerosene which are more economic and easily available than aircraft gasoline [21]. A typical efficiency value for a naturally aspirated 4-stroke SI engine is about 34% compared to almost 40% for a CI engine [22].

The usage of two-stroke technology together with advanced supercharging and injection systems, allows diesel engines to reach higher power densities at low rotational speeds, which are quite suitable for aircraft applications [21] because of the possibility of a direct connection to the propeller.

Accordingly, two stroke diesel engines have been considered in the present investigation as best today engine technology to compare conventional and hybrid electric configurations even if the approach can be extended to Wankel and turbine engines.

Let's consider a conventional non hybrid power system for a UAV whose propeller requires a brake mechanical power BHP_c to sustain flight at altitude z. The mass flow rate $G_{f,c}$ would be:

$$G_{f,c} = bsfc_c \cdot BHP_c \tag{2}$$

where $bsfc_c$ is the brake specific fuel consumption of the engine at that particular altitude and load. For a straightforward comparison with a hybrid electric power system, the specific endurance SE, i.e. the endurance per unit mass of fuel M_f, will be considered. At constant power, the specific endurance of a conventional non hybrid power system, SE_c, will be calculated as:

$$SE_c = \frac{1}{bsfc_c \cdot BHP_c} \tag{3}$$

For the proposed methodology, efficiency maps of the engine at sea level and in flight are needed. At each flight condition (altitude and power request), these maps are entered to obtain the *bsfc* of the engine. This allows a deep analysis of the engine working points, very important for the evaluation of fuel economy in hybrid electric power systems.

2.2 The electric machine

Liquid cooled permanent magnet brushless DC motors are considered here as representative of present-day technology. For this kind of machines, the peak or burst power can be assumed to be 2.5 times the nominal power [23].

For a specified motor technology, gravimetric and volumetric power densities and efficiency depend on the size and the speed of the machine. According to Snyder [24], the power density of existing electric motor is 3kW/kg (and is expected to increase up to 10kW/kg in the next 30 years). The efficiency of the electric machine increases with nominal power and rotational speed. Moreover, it is a function of the machine operating point (speed and load) and is different when it

works as a motor (η_M) or as a generator (η_G) [25]. Additionally, to take into account the whole electric drive (motor and inverter), the efficiency of the machine should be multiplied by the efficiency of the inverter, which increases with bus voltage [26].

2.3 The battery

Batteries are reversible electrical energy storage systems and limiting components of both electric and hybrid-electric aircraft. They are composed of a number of individual cells, each containing two electrodes and a medium that provides the ion transport between the two electrodes. Desirable attributes of batteries for propulsion are high specific power, high specific energy, long calendar and cycle life, high reliability and capacity to cope with low temperature environments.
The performance of a battery in terms of energy and power depends on the following nominal parameters that can be easily identified in its datasheet:

- The nominal capacity C that is measured in Ah and is evaluated by discharging the battery a specific constant current I_{nom};
- The number of cells in series (Ns) that, together with the rated voltage V_{cell}, defines the nominal voltage of the battery V_{nom} and the bus voltage of the power system.
- The maximum and cut-off voltage of the battery;
- The maximum current of the battery for continuous discharge, usually expressed as a multiple of the nominal capacity and named C_{rate}.
- The burst current. Each battery is also characterized by a C rating in terms of burst current, which measures how quickly the battery is able to discharge for a short time. This parameter is usually twice the C_{rate} [27] and will be named bC_{rate};
- The maximum recharge current which the battery can tolerate. It is also specified by the manufacturers as a multiple of the nominal capacity and will be denoted here as rC_{rate};
- The Depth of Discharge (DOD) is used to describe how deeply the battery can be discharged because a fully discharge (100% DOD) would shorten its cycle life.

According to these specifications, it is possible to calculate the nominal energy that can be drawn from a battery in discharging, $E_{d,nom}$, as:

$$E_{d,nom} = \frac{DOD}{100} \cdot C \cdot Ns \cdot V_{cell} \tag{4}$$

The nominal power that the battery can provide is:

$$P_{d,nom} = I_{nom} \cdot V_{nom} = C_{rate} \cdot C \cdot Ns \cdot V_{cell} \tag{5}$$

For a small amount of time (ranging from 10 to 30s) the battery is able to sustain the burst power:

$$P_{burst} = I_{burst} \cdot V_{nom} = bC_{rate} \cdot C \cdot Ns \cdot V_{cell} \tag{6}$$

The specific energy of a battery, also called gravimetric energy density or *GED*, is the amount of stored energy per unit mass, typically expressed in watt-hours per kilogram. In designing electric or hybrid electric aircraft, encumbrance is also a constraint because there is little room for battery packs, electric motor(s) and power control electronics. For this reason, the volumetric energy density of the battery, i.e. the amount of stored energy per unit volume, is also important.

At the moment, the best commercial technology in terms of gravimetric and volumetric energy density is represented by the lithium polymer cell even if other promising technologies are under investigation [1]. Lithium-polymer batteries will be henceforward referred to as “Li-po”.

A battery module is obtained by connecting a large number of cells in series and parallel, to achieve the desired values of bus voltage and capacity (energy). However, the mass of the battery pack is larger than the sum of cells in parallel and/or in series because of the presence of inter-cell connectors, separators infra-cell, control units, etc. that account for at least 30% of the final mass [6]. The additional mass is also larger when higher discharge currents are required. Consequently, the gravimetric energy density at battery-pack level is much lower than the cell specific energy and depends on C_{rate}, C and Ns. Being C and Ns the same, the higher the C_{rate}, the higher the battery

power. Therefore, using a pack with a higher C_{rate} will leave some room for extra power, safety, and extend the life of battery. On the other hand, batteries with higher C_{rate} are heavier and bulkier. Figure 2 shows the effect of C_{rate} on energy and power density of Li-po batteries according to the datasheet of different brands (namely Tattu, LiPol, Gens Ace and Polinovel). It is interesting to note that voltage has an effect on energy, power and mass if considered separately. On the other hand, energy and power densities of Li-po are only slightly affected by this parameter.

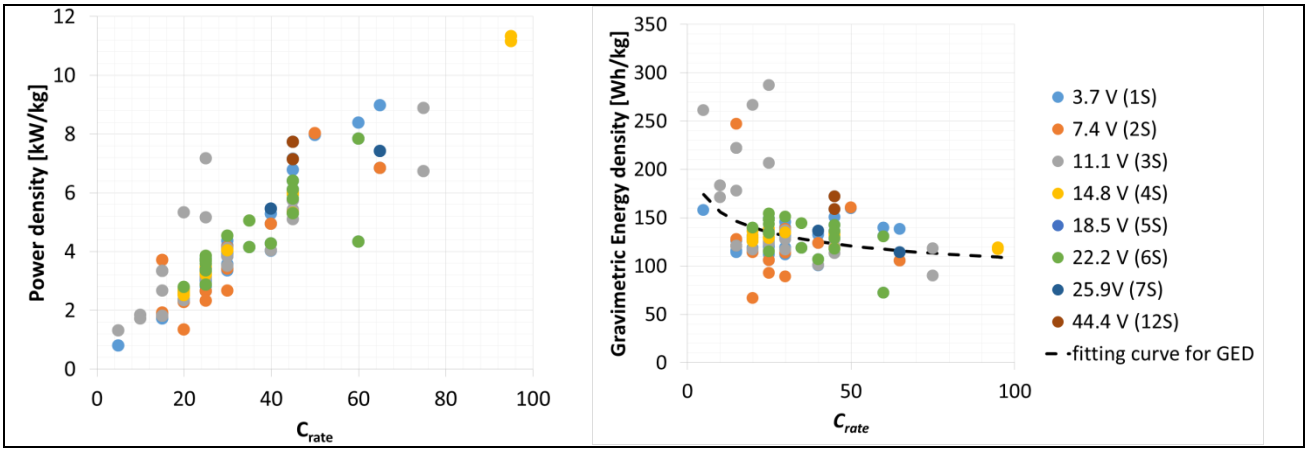

Figure 2 – Effect of C_{rate} rate on the energy and power density of Li-po batteries

To quantify the reduction of energy density with increasing C_{rate}, the following correlation was obtained by minimizing the Root Mean Squared Error from the data of Figure 2:

$$GED = 224.3 \cdot C_{rate}^{-0.158} \tag{7}$$

Note that this correlation is in accordance with [28], where the nominal energy density of a Li-po battery is reported to range between 110 and 170 Wh/kg and to be inversely proportional to power density.

3 Battery models

A battery can be modeled with an equivalent circuit consisting of an ideal open-circuit voltage source (OCV) in series with an internal resistance. By applying the Kirchoff's voltage law it is possible to write:

$$V(t) = OCV(t) - R(t) \cdot I(t) \tag{8}$$

The internal resistance *R* takes into account three contributions:

- The ohmic resistance;
- The charge-transfer resistance,
- The diffusion or concentration resistance.

The resistance depends on the battery state of charge and temperature [29], for this reason *R* is reported in eq. (8) as a function of the time. The open-circuit voltage also depends on the battery state of charge. In the Sheperd-Peukert model [30] the OCV is calculated as the sum of three terms: a constant voltage E_0, a polarization term and an exponential loss:

$$OCV(t) = E_0 - J\frac{C}{C - it}it + H\exp[-P \cdot it] \tag{9}$$

In this equation, $it = \int I(t)dt$ is the charge drawn from the battery at time *t* that can be also used to define the battery state of charge:

$$SOC = 100 \cdot \frac{C - it}{C} \tag{10}$$

The state of charge is the amount of charge remaining in the battery expressed as a percentage of its nominal capacity. It is the main state parameter in the control of hybrid electric power systems (see for example [31] and [32]).

The Sheperd-Peukert model was developed to simulate a typical constant-current discharge test that starts with the battery fully charged (SOC=100%, battery voltage equals the open-circuit voltage). A constant current is then applied and the battery voltage starts to decrease. After a certain time, the cut-off voltage is recharged and the battery is considered discharged. The battery discharge time t_d depends on the discharge current but the dependence is not of inverse proportionality due to the so-called Peukert effect [25]:

$$t_d = const \cdot I^{-n} \tag{11}$$

The Peukert coefficient n depends on the cell technology and varies between 1 and 1.5 [33]. As a consequence of the Peukert effect, the capacity of the battery is a function of the discharge current:

$$C = const \cdot I^{1-n} \tag{12}$$

The capacity reduction that occurs at high discharging currents is an important issue often neglected in the sizing and analysis of electric and hybrid powertrains as in [34].

The maximum current that can be delivered by the battery [25] is:

$$I_{\max} = \frac{OCV(t)}{2R(t)} \tag{13}$$

In practice the battery voltage is limited to a narrow band around *OCV*. Considering the minimum battery voltage, the maximum current can be calculated as [25]:

$$I_{\max} = \frac{OCV - V_{\min}}{2R} \tag{14}$$

When the battery is fully charged, according to the Sheperd-Peukert Model, $OCV = E_0 + H$. This equation allows the internal resistance to be correlated to the bC_{rate} of the battery:

$$R = \frac{E_0 + H - V_{\min}}{2 \cdot bC_{rate} \cdot C} \tag{15}$$

The nominal specifications of a Li-po cell as found in literature [6, 8, 35- 36] are summarized in Table 2.

Table 2 – Specifications of the Lithium-Polymer cell

Parameters	**Symbol**	**Lithium-Polymer**
Rated Voltage [V]	V_{cell}	3.7
Max Voltage [V]	V_{max}	4.2
Cut-off Voltage [V]	V_{min}	2.7
Operating temperature [°C]		-20/60
Peukert coefficient	n	1.05
Depth of Discharge [%]	DOD	80%

Two different set of values for E_0, J and H were proposed in literature for Li-po batteries by fitting experimental constant current discharge curves and are reported in Table 3. The authors noted that both sets of values give similar values of $Eo+H$ and that these values are practically equal to the maximum voltage V_{max} of a Li-po cell.

Table 3 – Literature values for the parameters of the battery model

Ref.	**E_0**	**H**	**E_0+H**
Arista et al. 2015 [6]	3.694	0.5458	4.24
Tremblay et al. 2009 [30]	3.508	0.6231	4.13

Accordingly, the authors propose to express the internal resistance as:

$$R = \frac{V_{\max} - V_{\min}}{2 \cdot bC_{rate} \cdot C} \tag{16}$$

Therefore, R is assumed to be independent of the battery state of charge in the present investigation. In this way, the internal resistance is estimated as a function of rate parameters that can be easily found in the datasheets of the batteries.

3.1 Constant power discharge models

The power to be delivered by the battery in case of constant speed–steady level electric flight, P_{batt}, is:

$$P_{batt} = \frac{BHP}{\eta_M} \tag{17}$$

where η_M is the overall efficiency of the electric drive (motor and driver) [3].

In 2011, Traub [3] proposed the following formula to evaluate the endurance of electric flight:

$$t_{d,T} = \left(\frac{I_{nom}}{C}\right)^{1-n} \left(\frac{n_s V_{cell} \cdot C}{P_{batt}}\right)^{n} \tag{18}$$

Note that endurance and discharge time can be considered as synonyms in the case of constant power electric flight.

More recently, Traub [7] analyzed the validity of eq. (18) by considering six tests at constant power using two Li-po batteries with different nominal capacity. He found an average error of 22% and tried to reduce the error by considering the average battery voltage instead of the nominal one and by adjusting the Peukert coefficient.

According to the authors of the present investigation, the Traub formula is valid but has some limits:

1) It does not take into account that the battery is not able to sustain a constant power request below a certain state of charge;

2) It cannot be applied to hybrid electric aircraft where the battery could not be fully charged at the beginning of the electric flight (SOC_{in}<100%) or fully discharged at the end (SOC_{fin}>20%).

3) It does not put in evidence the technological limits of the battery and in particular its maximum power.

A modified version of the Traub formula is proposed here to address these issues:

$$t_{d,mT} = R_t^{1-n} \left(\frac{SOC_{in} - SOC_{fin}}{L \cdot bC_{rate}}\right)^{n} \tag{19}$$

Where *L* is load of the battery is defined as the percentage of the battery maximum power drawn from the battery:

$$L = \frac{P_{batt}}{P_{burst}} \cdot 100 = \frac{P_{batt}}{bC_{rate} \cdot C \cdot N_s \cdot V_{cell}} \cdot 100 \tag{20}$$

Note that eq. (19) is identical to the Traub formula, eq. (18), if SOC_{in}=100% and SOC_{fin}=0 but puts into evidence the load of the battery and allows a direct comparison with the Ragone method proposed by Christen et al. [11].

Using the electric circuit equivalent explained in the previous section, the Ragone model calculates the battery current as:

$$I\ (P_{batt}) = \frac{OCV}{2R} - \sqrt{\frac{OCV^2}{4R^2} - \frac{P_{batt}}{R}} \tag{21}$$

The energy that the battery is actually able to release at a specific power P_{batt} is given by:

$$E_d(P_{batt}) = \frac{2R \cdot C \cdot P_{batt}}{OCV - \sqrt{OCV^2 - 4RP_{batt}}} \tag{22}$$

At the endpoint of the Ragone curve (P_{batt}=P_{burst}) only half of the energy is available while the other half is lost at the internal resistance. The discharge time at each value of P_{batt} can be calculated with the Ragone approach as E_b/P_{batt}:

$$t_{d,R}(P_{batt}) = \frac{C}{I(P_{batt})} = \frac{2R \cdot C}{OCV - \sqrt{OCV^2 - 4RP_{batt}}} \tag{23}$$

This approach, however, does not take into account the Peukert effect, i.e. the capacity of the battery is assumed equal to the nominal value C independently of the power required to the battery. To take into account the Peukert effect, eq. (23) was modified in the present investigation by using the effective current I_{eff} [37] instead of the actual battery current:

$$I_{eff} = I\left(\frac{I}{I_{nom}}\right)^{n-1} \tag{24}$$

Therefore, the discharge time is calculated with the modified Ragone model as:

$$t_{d,mR}(P_{batt}) = \frac{C}{I_{eff}} \tag{25}$$

The logarithmic plots of Figure 3 show the reduction of battery energy due to the Peukert effect on a dimensionless Ragone plot.

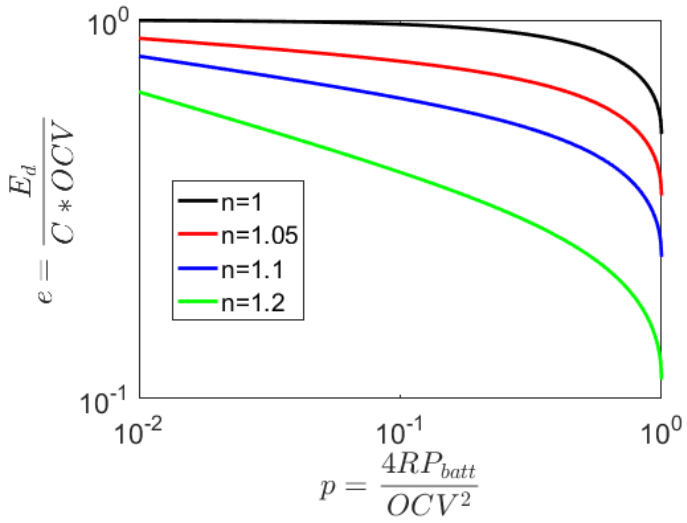

Figure 3 – Correction to dimensionless Ragone plot to account for Peukert effect

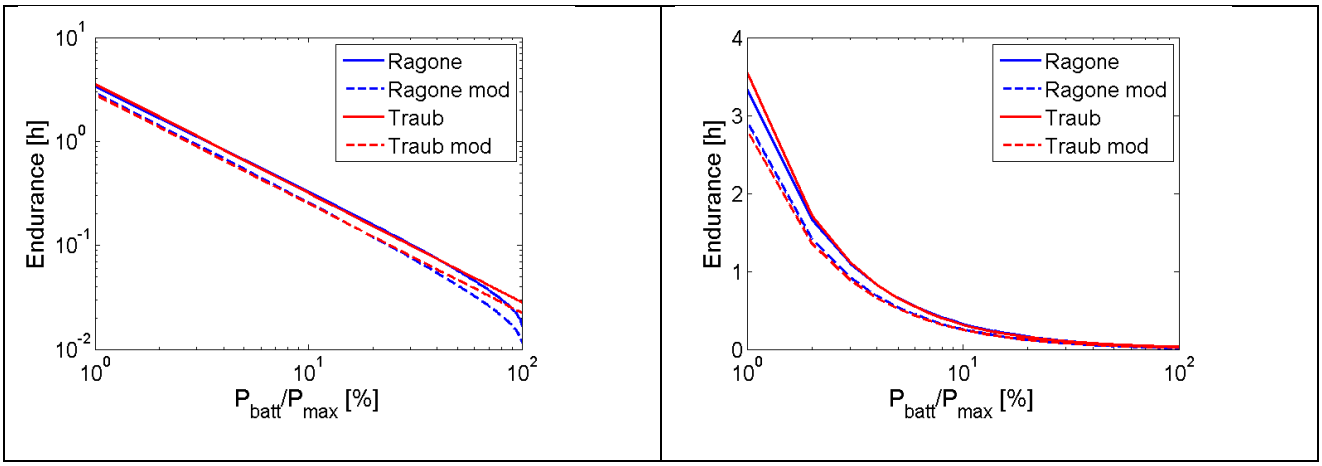

Figure 4 – Discharge time/endurance versus battery load with the proposed equations

Figure 4 compares the results of equations (18), (19), (23) and (25) with different axis scales. Note that the original Ragone approach eq. (23) and the Traub formula eq. (18) give almost the same results with small differences only for very low (P_{batt}/P_{max}<1%) or very high (P_{batt}/P_{max}>25%) values of the loads. The proposed amended models predict a lower endurance/discharge time than the original ones.

3.2 Experimental validation of the discharge models

The validity of the proposed modified approaches has been verified by comparing the calculated discharge time with the experimental data of electric endurance found in literature [7,8] and reported in Table 4.

To measure the endurance of an electric aircraft, Traub [7] built a radio controlled electric UAV and tested it in a wind tunnel. After setting the tunnel to the selected velocity, power to the electric motor was increased until the propeller thrust equaled the aircraft drag. Power, voltage and current were monitored until steady level flight was no more achievable at the set flight speed. This condition was used to define the electric endurance at that flight speed. The experimental data of Avanzini et al. [8] were obtained by means of an electronic load applied to Li-po batteries to simulate the discharge at different power levels starting form a fully charged condition.

Table 4 – Experimental discharge times available in literature

Test	C	N_s	C_{rate}	bC_{rate}	P_{nom}	P_{burst}	$P_{batt,\ test}$	t_d	*Ref.*
	[Ah]		[A]	[A]	[W]	[W]	[W]	[h]	
1	0.5	3	20C	30C	81.0	121.5	18.4	0.2250	Traub (2013) [7]
2							19.5	0.2290	
3							35.2	0.1170	
4	0.75	1	20C	40C	40.5	81.0	2.5	0.9201	Avanzini et al. (2016) [8]
5							5.0	0.4497	
6							10	0.2159	
7							15	0.1363	
4	1.0	3	20C	30C	162	243	20.5	0.4660	Traub (2013) [7]
5							22.1	0.3750	
6							32.2	0.2670	
11	2.5	2	20C	40C	270	540	10	1.5212	Avanzini et al. (2016) [8]
12							20	0.7447	
13							40	0.3576	
14							60	0.2330	
15	5.0	6	20C	40C	1620	3240	50	1.8451	Avanzini et al. (2016) [8]
16							100	0.9176	
17							200	0.4540	
18							300	0.3001	
19	5.4	4	20C	40C	1166	2332	50	1.3193	Avanzini et al. (2016) [8]
20							100	0.6502	
21							200	0.3219	
22							300	0.2056	

The results of the comparison are shown in Figure 5. Note that a logarithmic scale is used for the load that never exceeds 20% in the experimental tests.

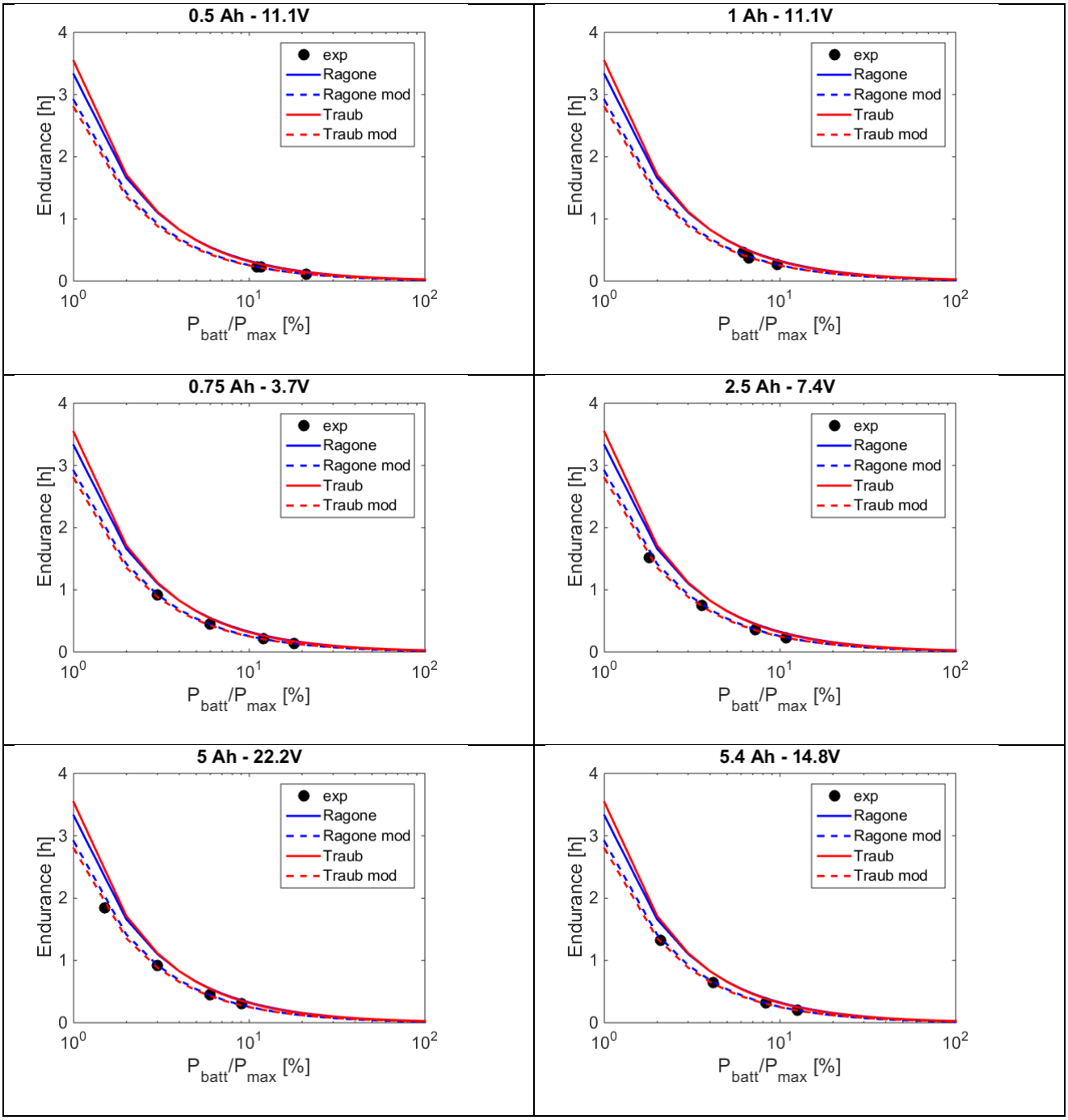

Figure 5 – Validation of the proposed formulas for discharge time/endurance with experimental data

The absolute and relative errors with the proposed formulas are compared with the original Traub and Ragone approaches in Figure 6 and Figure 7.

The absolute error with both modified formulas is below 5 minutes for all tests. As for the relative errors, Figure 7, the proposed correction to Traub formula allows a reduction of the average relative error from 22% to 4%. The amendment to Ragone approach reduces the average error from 9 to 3%. This stresses the importance of considering both the technical limits of the battery (DOD, maximum power, etc.) and the Peukert effect when modeling the battery discharge time.

Overall, the modified Ragone approach is the most accurate but the modified Traub formula is easier to use. For this reason it will be used in the test case reported later in the paper.

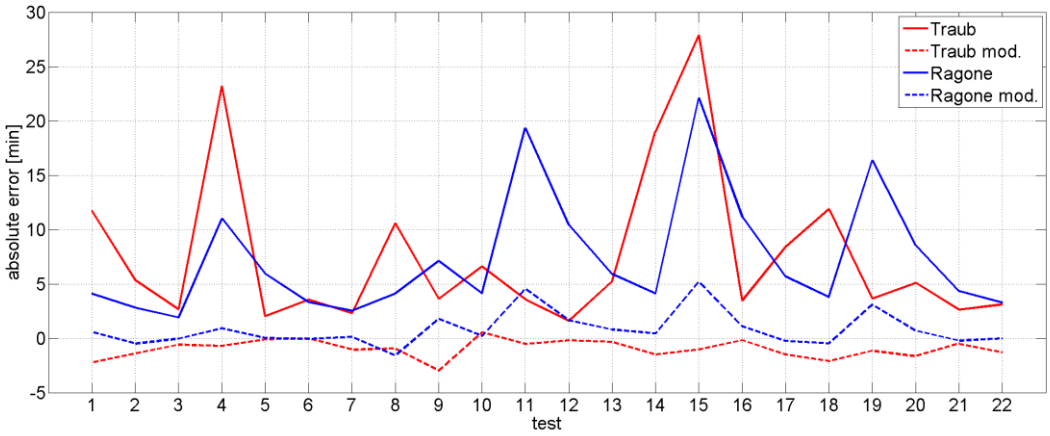

Figure 6 – Absolute relative errors of the proposed formulas for discharge time

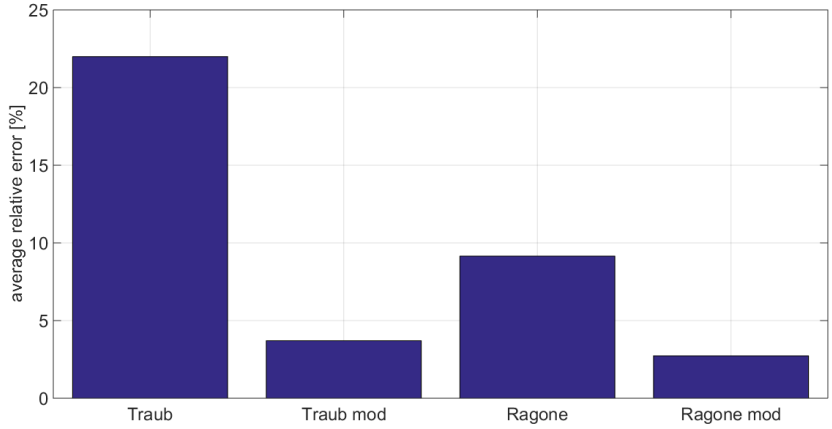

Figure 7 – Average relative errors of the proposed formulas for discharge time

3.3 Battery charging models

For the design and management of hybrid electric power systems it is necessary to evaluate the time and the power required for charging the battery. In hybrid electric power systems, batteries are usually recharged on board using the engine/alternator and different charging schemes can be used. This means that they are not necessarily charged at the rC_{rate} specified by the manufacturers. Moreover, the charging current may not be kept constant during charge. In fact, the goal of the charger is not only getting back as much as possible charge in the battery but also knowing when to stop to avoid damages and maintain the temperature within its safe limits [38]. This is usually performed by limiting the voltage of the battery within a termination value.

Among the different schemes for fast charging, the constant-current constant-voltage (CC/CV) method is preferred for Lithium batteries. In this method, charging is started at constant current I_0 and switches to constant voltage before the cell voltage reaches its upper limit. In the first step (whose duration will be denoted as t_{CC}), the voltage rapidly goes up until the upper voltage limit of the cell is reached. This limit should be equal to V_{max}=4.2 V for all lithium batteries; however, lithium batteries are sometimes charged to 4.1V to increase the cycle life even if this reduces the effective cell capacity by about 10% [39]. During the CC charge, the power needed for the charge increases with time.

When the upper voltage limit is reached, the state of charge of the battery is less than 100%. To restore the initial capacity, a constant voltage recharge is performed for a time t_{CV}. The current decreases exponentially up to a cut off current that can be set in the range 0.03 I_0-0.1I_0 [40, 41]. When using complex recharging schemes, it is not possible to estimate the time to charge a battery by simply dividing the nominal capacity of the battery by the specified charging rC_{rate}.

For this reason model has been developed in the present investigation to calculate the charging time as the sum of t_{CC} and t_{CV} that in turns are a function of I_0, initial state of charge SOC_{in}, desired final state of charge $SOC_{fin.}$, cut off current (defined as kI_0) and upper voltage limit V_{max}.

Since SOC increases linearly during the CC phase starting from SOC_{in} to SOC_{CC}, it is possible to calculate t_{CC} as:

$$t_{CC} = \frac{SOC_{CC} - SOC_{in}}{100} \cdot \frac{C}{I_0} \tag{26}$$

As said before, the SOC_{CC} at the end of the first step is lower than 100%. It can be either assumed or calculated from experimental values of voltage at the end of the first step:

$$V(t_{CC}) = OCV(SOC_{CC}) + RI_0 = V_{\max} \tag{27}$$

As already explained, the open circuit voltage is a function of the *SOC*. However, the correlation between measured battery open circuit voltage and *SOC* is uncertain for Lithium batteries, mainly for two reasons [29]. The first one is that the *OCV* versus *SOC* curve has a very low slope. The second one is that *OCV* depends also on the temperature of the battery. Figure 8 compares four different *OCV* vs *SOC* curves retrieved in literature [6,29,42,43] for Li-po batteries

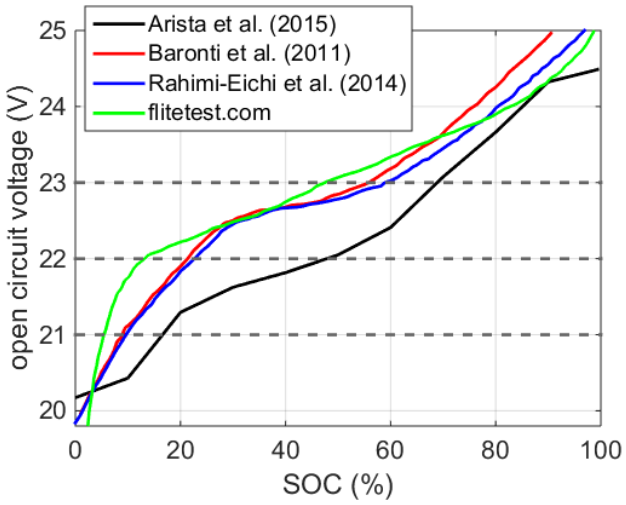

Figure 8 – Estimated open circuit voltage versus state of charge for a 6S lithium-polymer battery

The charge current in the CV phase can be modelled as:

$$I(t) = I_0 e^{-h(t-t_{CC})} \tag{28}$$

where the parameter *h* has to be calculated by imposing two conditions.

The first condition is on the selected cut off current that is reached at time $t_{CV}+t_{CC}$:

$$I(t_{CV}+t_{CC}) = I_0 e^{-ht_{CV}} = \frac{I_0}{\frac{1}{k}} \Rightarrow h = \frac{\log\frac{1}{k}}{t_{cv}} \tag{29}$$

Hence, in the second step the charge current becomes:

$$I(t) = I_0 e^{-\frac{\log\frac{1}{k}}{t_{CV}}(t-t_{CC})} \tag{30}$$

The second condition is that the area under the current curve in the CV phase has to match the desired final state of charge SOC_{fin}.

$$\frac{SOC_{cc}}{100} + \frac{I_0}{C}\int_{t_{CC}}^{t_{CC}+t_{CV}} e^{-\frac{\log\frac{1}{k}}{t_{CV}}(t-t_{CC})}\,dt = \frac{SOC_{fin}}{100} \tag{31}$$

Solving the definite integral, a formula for t_{CV} is obtained:

$$t_{CV} = \left[\frac{SOC_{fin}-SOC_{in}}{100}\cdot\frac{C}{I_0} - t_{CC}\right]\cdot\frac{\log\frac{1}{k}}{1-k} \tag{32}$$

By substituting eq. (26) in eq. (32), it is also possible to write:

$$t_{CV} = \left[\frac{SOC_{fin}-SOC_{CC}}{100}\cdot\frac{C}{I_0}\right]\cdot\frac{\log\frac{1}{k}}{1-k} \tag{33}$$

The total charge time is:

$$t_r = t_{CC} + t_{CV} \tag{34}$$

By multiplying the voltage and the current of the two phases of the charge it is possible to obtain the battery charging power and, by integration, the corresponding energy E_r. The corresponding formulas are reported in appendix.

3.4 Experimental validation of the proposed charging model

The only experimental data found in literature about the charging process of Li-po batteries were those of Verstraete et al. [12] that include current and voltage curves for two batteries with different capacity but with the same C_{rate} and N_s and are summarized in Table 5. The first three tests were carried out with a 6S 1350-mAh Li-Poly battery (initial open circuit voltage OCV_{in} equal to 21V, 22V and 23V respectively) and the fourth test with 6S 2100-mAh Li-Poly battery (OCV_{in} =22V).

In each test a current I_0 = 0.85-0.9 A is used in the CC charge. The CV phase is started when a voltage of 24.2 V is reached. This upper voltage corresponds to a SOC of about 70% [12].

The initial state of the charge was estimated using the correlation of Baronti et al. [29] shown in Figure 8. The final state of the charge was estimated with the Coulomb counting method applied to the experimental values of current during the CV phase [44]. For more details about the estimation of the SOC please refers to [9].

Table 5 – Experimental data for the validation of the charging model

Test	*C*	OCV_{in} [V]	I_0 [A]	SOC_{in}	I_{fin}	SOC_{fin}	t_s *[h]*	E_s *[Wh]*
1	1.35	21	0.85	8%	0.1 I_0	80%	1.53	20.8
2	1.35	22	0.9	19%	0.1 I_0	80%	1.38	20.0
3	1.35	23	0.9	56%	0.1 I_0	80%	0.76	8.53
4	2.1	21	0.9	19%	0.1 I_0	80%	2.03	33.2

The comparison between the proposed charging model and the experimental values of current and voltage is shown in Figure 9. It can be noticed that the model predicts with reasonable accuracy the time histories of both current and voltage.

However, for the purpose of the model, it is important to capture the time and the energy required to charge the battery (Figure 10). The errors committed with the model are below 7% and 10% for time and energy, respectively.

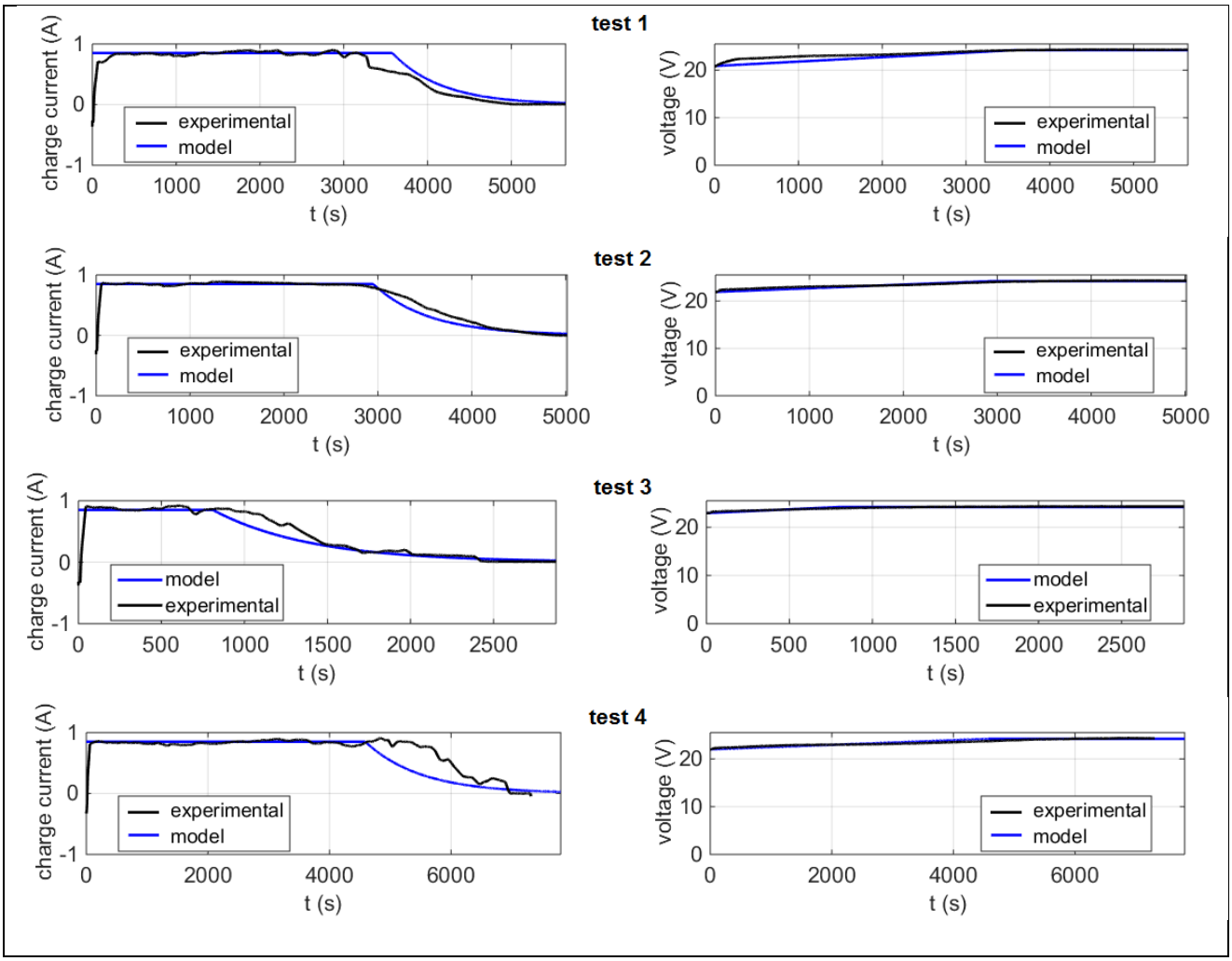

Figure 9 –Experimental and numerical time histories of current and voltage during battery charge

The uncertainty on the open circuit voltage (Figure 8) strongly affects the validation. For this reason, an uncertainty bar is reported in the figure. Specific tests will be performed as further investigation to validate the proposed model under controlled charge processes.

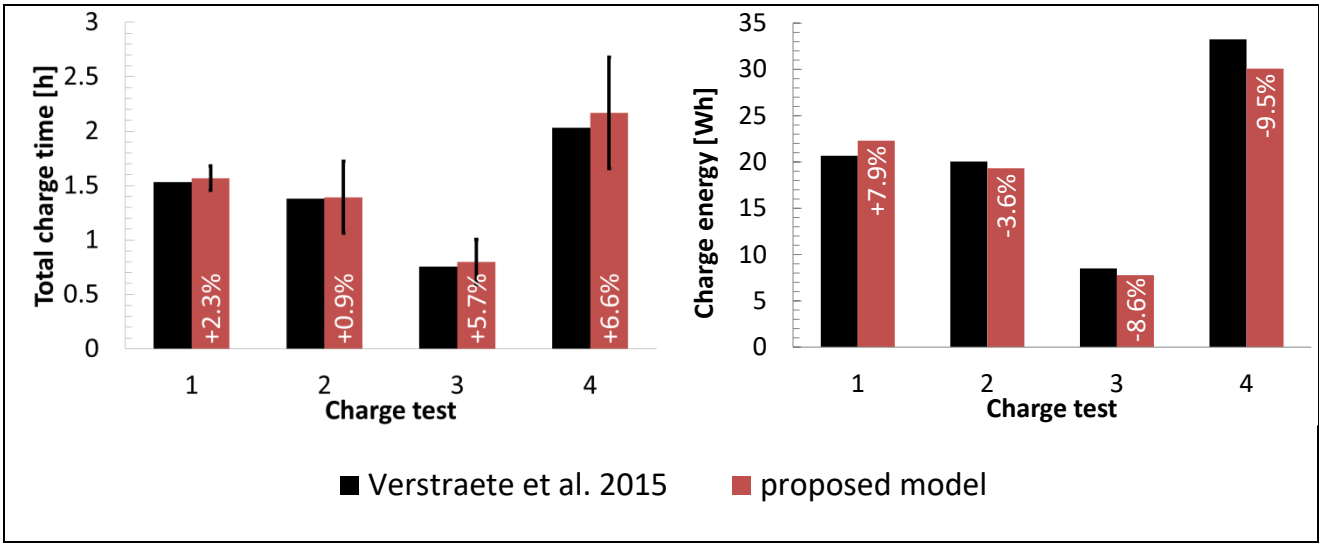

Figure 10 – Validation of the proposed mode for charge time and energy (uncertainty bar showing the uncertainty in the initial SOC)

4 Endurance of hybrid electric aircraft

A parallel hybrid electric power system (Figure 1) with five possible operating modes was considered to propose a methodology for evaluating the endurance of a hybrid electric power system.

For about 30s both the motor and the battery can sustain very high currents. This allows the definition of a Mode 0 where the battery and the motor works at their peak power [21]. This operating mode can be used for a faster and safer takeoff. In thermal mode (Mode 1), the engine produces all the power required by the propeller while the electric drive is not used. In electric flight (Mode 2), the required BHP is generated by the motor using the battery as only energy source and the engine is turned off. The charging mode is named mode 3: the engine generates the power required to move the propeller and to charge the battery while the electric motor works as a generator. Finally, both the engine and the motor are used to generate the required BHP in Mode 4. The usage of these operating modes along the mission needs to be optimized according to the mission of the aircraft. The Airbus Group [45] the usage of Mode 2 for takeoff, climb, descent and landing in civil aircraft, while the cruise should be performed in Mode 3. The present investigation considers a UAV in steady flight conditions (loiter). A goal of the hybridization in this application is the possibility of flying as long as possible in electric mode. Therefore, the battery discharge time t_d that coincides with the electric endurance *EE*, will be set as first key performance index. In the case of the conventional non hybrid power system, the electric endurance is zero.

Loiter is supposed be performed in two possible ways:

(1) Always in Mode 1 (thermal);

(2) Swapping between Mode 2 and Mode 3 (ON-OFF strategy).

If the first case, the fuel flow rate can be calculated in the same way as in the conventional case:

$$G_{f,t} = bsfc_t \cdot BHP_h \tag{35}$$

In this equation, $bsfc_t$ is the specific fuel consumption of the engine when the power system works at mode 1. BHP_h is the brake specific horse power required to sustain the hybrid electric aircraft at altitude z. Note that it expected to be higher than BHP_c in eq. (2) due to the different mass of the hybrid electric power system. The engine operating point, and therefore $bsfc_t$, is also likely to be different from the conventional case.

The potential improvement in fuel consumption assured by the hybrid configurations could be used either to increase the payload (by reducing the mass of fuel on-board) or to increase the overall endurance. On the contrary, a hypothetical increase of fuel consumption due to the larger mass could decrease the payload or the overall endurance. To include both cases, the authors propose the use of specific endurance performance index for the comparison. In the thermal case, it is calculated, similarly to the conventional case, as:

$$SE_t = \frac{1}{bsfc_t \cdot BHP_h} \tag{36}$$

In the ON-OFF strategy, the battery state of the charge is allowed to vary between SOC_{inf} and SOC_{sup}. These thresholds can be selected by the energy manager together with the recharge current I_0 and the cut off parameter k. Therefore, the engine is turned alternatively OFF for t_d hours (mode=2) and ON for t_r hours (mode=3) where t_d is calculated by eq. (19) by assuming $SOC_{fin}=SOC_{inf}$ and $SOC_{in}=SOC_{sup}$. The battery load is calculated as:

$$L = \frac{BHP_h}{\eta_M \cdot (C \cdot N_s \cdot V_{nom} \cdot bC_{rate})} \cdot 100 \tag{37}$$

The recharge time is calculated with equations (33)-(34) where $SOC_{fin}=SOC_{sup}$ and $SOC_{in}=SOC_{inf}$. When turned off, the fuel flow rate is zero. When turned on, the engine works at a different operating point than in the thermal strategy because it has to generate both the propeller brake power and the battery recharge power $P_{r,max}$. The corresponding brake specific fuel consumption will be named $bsfc_r$.

The fuel consumed in a cycle of t_d+t_r hours with the ON-OFF strategy can be calculated as:

$$G_{f,r} = \frac{bsfc_r \cdot \left(BHP_h \cdot t_r + \frac{E_r}{\eta_G} \right)}{t_d + t_r} \tag{38}$$

while in the specific endurance is given by:

$$SE_{ON-OFF} = \frac{(t_r + t_d)}{bsfc_r \cdot \left(BHP_h \cdot t_r + \frac{E_r}{\eta_G} \right)} [h/kg] \tag{39}$$

This is the final formula proposed in the present investigation for the evaluation of endurance in a parallel hybrid electric power system with an ON-OFF energy management strategy.

5 Test case

A hypothetical UAV similar to the Galileo Avionica Falco is employed as a test case to show how the proposed methodology can be used for real applications. The specifications of the UAV are reported in Table 6.

Table 6 – Specifications of the UAV used as a test case

	Unit	**Value**
Initial takeoff mass	kg	500
Wing load (*W/S*)	kg/m^2	64
C_{D0}		0.025
K		0.08
U (loiter)	m/s	40
Altitude (loiter)	m	4200
Thrust horse power (*THP*)	kW	8.8
η_P		0.8
Brake power at loiter (BHP_c)	kW	11
Engine rated power	kW	60

A two-stroke diesel engine with a nominal power of 60kW and a constant speed of 2400 rpm is considered for both the conventional and the hybrid electric configurations. The efficiency maps at sea level and in flight have been obtained by applying a scaling procedure for two stroke diesel engines proposed in a previous investigation [46] and will be shown in section 6.

Note that the brake power in cruise is only 18% of the engine rated power. This guarantees excess power for climb and acceleration and allows a safe and fast takeoff. However, working at 18% of its nominal power causes the engine to perform very poorly in terms of fuel efficiency. In fact, the $bsfc_c$ of the two stroke diesel engine in the non-hybrid case is 440g/kWh as shown in section 6. Therefore, the specific endurance SE_c calculated with eq. (2) is 0.19 h/kg.

Using this configuration as a baseline case, a hybrid electric power system is sized and analyzed with both strategies considered in the previous section: thermal and ON-OFF.

In the ON-OFF strategy, the battery is discharged from SOC_{sup}=90% to SOC_{inf}=20% (Mode 2) and then recharged again up to SOC_{sup} in Mode 3. The input parameters of the ON-OFF strategy are reported in Table 7.

The electric machine works as a motor in mode 2 and as a generator in mode 3. Since a scalable performance map of a motor for aircraft application is not easy to find, the efficiency of the electric machine is considered the same in the two modes ($\eta_M = \eta_G$) and equal to 0.9 [24].

Table 7 – Specification of the ON-OFF energy SOC_{inf} management strategy

	Unit	Value
SOC_{sup}	%	90
SOC_{inf}	%	20
SOC_{cc}	%	70
I_0	A	1C
k		0.03

5.1 Sizing of the batteries

The batteries were sized according to the first performance index, i.e. the electric endurance. The minimum battery capacity able to meet the request of electric power, BHP/η_M for a selected minimum time (30, 60 and 90 minutes) was calculated with the recursive procedure here explained. The procedure starts from the initial weight of the aircraft (Table 6) and calculates the nominal capacity of the battery required to power the aircraft for the selected time. The corresponding battery mass is calculated using the gravimetric energy density of eq. (7). Specific power could be used instead of C_{rate} in this sizing procedure. However, the authors preferred to use the C_{rate} because this is a parameter that can be easily found in a battery datasheet. For the proposed application, 73 cells in series have been considered to reach the total nominal voltage of 270V as suggested by Bérubé et al. [47].

Then, aircraft weight is increased to allow for the presence of the battery. The empty mass and the wing area are re-calculated assuming, for the wing area, a constant wing loading. The empty mass is upgraded with the following correlations derived from Panagiotou et al. [48]:

$$W_E = 0.92 W_{to}^{-0.8} \tag{40}$$

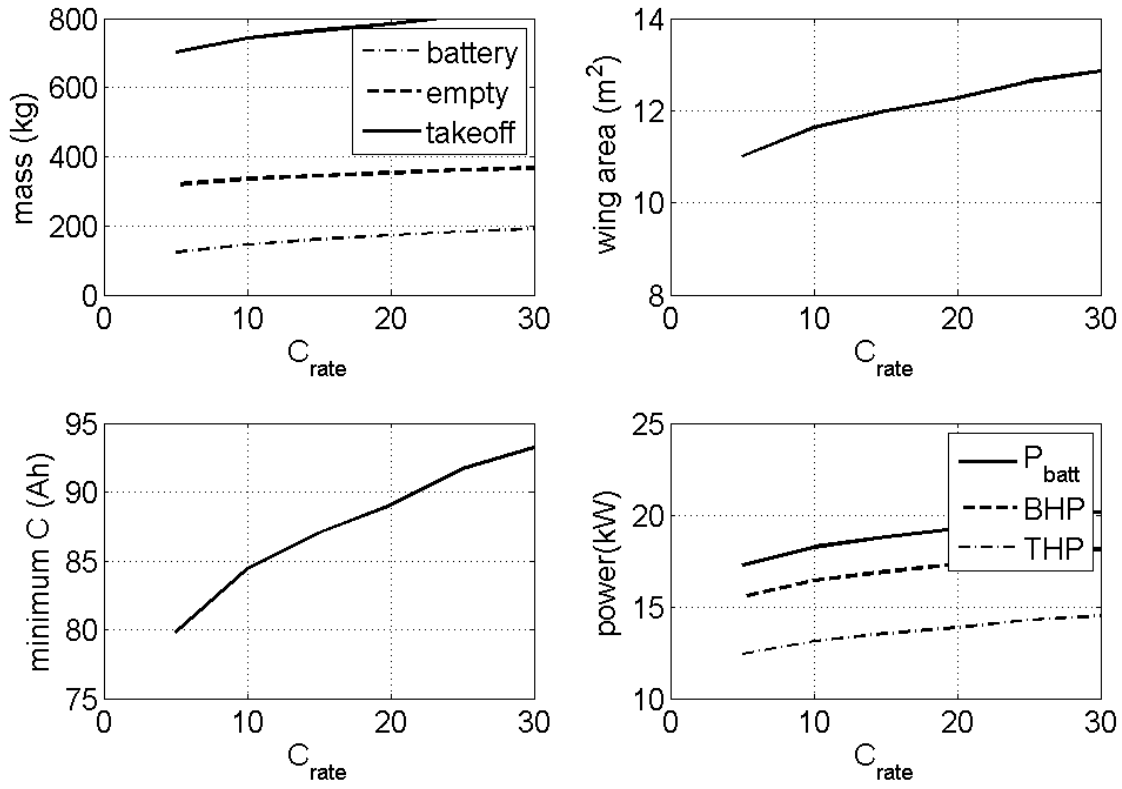

Figure 11 – Results of the sizing procedure for 1 h of electric flight

The procedure is repeated until reaching convergence. The minimum capacity required for a flight time of 1h when C_{rate} is increased from 5C to 30C is shown in the bottom left plot of Figure 11. The trends of battery, empty and takeoff masses as a function of C_{rate} are presented in the top left plot of Figure 11. The corresponding wing areas are displayed in the top right plot. The bottom right plot of Figure 11 shows the required values of THP, BHP and P_{batt} versus C_{rate}.

The capacity of the battery needs to be increased from 80to 93Ah when C_{rate} is increased from 5C to 30C to allow an hour of flight in electric mode. This causes a significant increase of the aircraft weight and of the power needed to propel the aircraft. Thanks to the better gravimetric density, the

batteries with the lower C_{rate} give the best results. Actually, the nominal C_{rate} could be furtherly decreased for this kind of application.

Table 8 summarizes the specification of the batteries required for an electric endurance of 0.5, 1 and 1.5h, respectively, with a C_{rate} of 5C.. For each battery, the time, the power and the energy required for a recharge from SOC_{inf} to SOC_{sup} are also reported. Note that the recharge time is the same for all batteries because the same charging current is used in the three cases. On the other hand, charging power and the energy linearly increase with the battery capacity.

Table 8 – Specification of the batteries for 0.5, 1 and 1.5 hours in electric flight

		Battery 1	Battery 2	Battery 3
EE	h	0.5	1.0	1.5
C	Ah	34.5	80	146
N_s		73	73	73
C_{rate}		5C	5C	5C
I_0	A	34.5 (1C)	80 (1C)	146(1C)
t_r	h	1.58	1.58	1.58
P_r	kW	9.8	23	42.6
E_r	kWh	7.6	17.9	33.1

5.2 Sizing of the electric machine

The electric machine works as a motor in Mode 2 and as a generator in Mode 3 in the ON-OFF strategy. Therefore, its nominal power $P_{M,nom}$ is calculated as the maximum between the power required to sustain loiter, BHP_h, and P_r/η_G.

Considering the state of the art, the power density of the motor was set equal to 3kW/kg as suggested by Snyder [24]. The additional mass of the electric drive (motor + driver) can be neglected in the iterative procedure, being about 16 kg in the worst case and well below the battery mass. Moreover, Olsen et al. [49] pointed out that the use of a powerful electric machine in hybrid electric power systems negates the need for the conventional small starter/generator machine and the large battery required by the hybrid powertrain denies the need for a small conventional battery.

The masses of these removed components could easily account for the additional masses of the electric machines reported in Table 9.

The degree of hybridization, i.e. the power of the motor divided by the total power (motor + engine), is obtained as a result of the proposed sizing procedure. Note that the degree of hybridization at cruise is different from that at takeoff.

At takeoff, the engine delivers its nominal power and the motor can work at burst power for a short amount of time (Mode 0). The burst power can be assumed equal to twice the nominal one as in the case of batteries.

At cruise, the engine produces less power due to the altitude effects while the motor works at its nominal power.

Accordingly, a different degree of hybridization can be defined at cruise:

$$HD = \frac{\mathrm{P_{M,nom}}}{\mathrm{P_{ICE,cruise}} + \mathrm{P_{M,nom}}} \tag{41}$$

And at takeoff (sea level):

$$HD_{to} = \frac{2P_{M,nom}}{P_{ICE,sl} + 2P_{M,nom}} \tag{42}$$

The values of both hybridization degrees for the proposed configuration are reported in Table 9.

Table 9 – Results of the motor sizing

		Battery 1	Battery 2	Battery 3
Nominal power	kW	14.1	25.6	47.3
Mass	kg	4.8	8.5	15.8
Efficiency		0.9	0.9	0.9
hybridization degree (cruise)		21%	32%	47%
hybridization degree (takeoff)		32%	46%	61%

In consequence of the energy density of Li-po battery, the hybrid electric configurations with batteries 1, 2 and 3 require takeoff mass to be increased by 18%, 20% and 25% with respect to the baseline non-hybrid case. The details of the mass of the proposed configurations are shown in Figure 12.

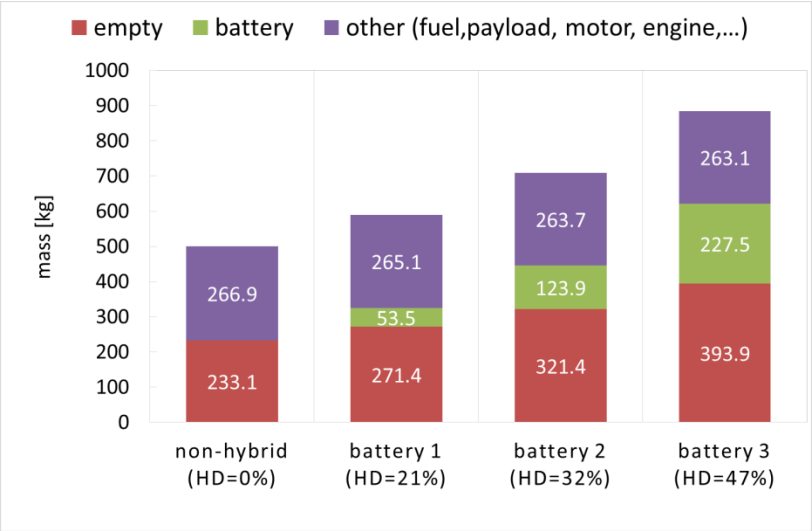

Figure 12 – Distribution of mass in the proposed powertrains with increasing hybridization degree

6 Results and discussion

In this section, the specific endurance of the conventional non hybrid case, eq. (3), is compared with the SE of the three different hybrid powertrains with increasing hybridization degree (battery 1, 2 and 3). The required BHP is computed with the masses of Figure 12. For each hybrid case, the specific endurance is calculated with both energy management strategies considered in Section 4, i.e. thermal and ON-OFF. Therefore, a total of 7 cases are considered and the engine operating mode in each case is evaluated with the performance map for the two stroke diesel engine with a nominal power of 60kW and a constant speed of 2400rpm.

The operating points of the engine in thermal mode are displayed in Figure 13a together with the conventional non hybrid case. For the conventional configuration, the working point is found by entering the altitude and brake power reported in Table 6, i.e. with reference to the initial mass of the UAV. For the hybrid electric configurations, the altitude is the same but BHP_h is higher because of the larger mass of the aircraft (Figure 12). In particular, it is 14.4, 16 and 21.5 kW for batteries 1, 2 and 3, respectively. Note that in all cases, the engine is able to generate a power much higher than BHP. This excess power could be used for maneuvers.

As shown in Figure 13a, bsf_c is 480 g/kWh in the non-hybrid case while and bsf_t decreases from 420 to 353 g/kWh when the hybridization degree increases from 21% to 47%.

Note that fuel flow rate in eq. (35) is obtained in the hypothesis of constant brake power during cruise. Actually, the weight of the aircraft decreases during this phase, so BHP also decreases and

bsfc increases. However, it is possible to simplify the analysis by assuming their product to be constant.

In the ON-OFF strategy operating mode, the engine is turned alternatively OFF for t_d hours and ON for t_r hours. When turned OFF, the engine fuel consumption is zero. When turned ON, the engine works at the operating points shown in Figure 13b. In this case, it is used to generate both the BHP required for the flight and the power P_r needed to recharge the battery recharge (Table 8). Note that the $bsfc_r$ of the engine is 315 g/kWh for battery 1 and 275 g/kWh for battery 2. The engine is not able to recharge battery 3 at the selected current I_0 because this would require a power higher than 54kW, i.e. the maximum power that the engine is able to generate at the loiter altitude. However, the battery could be recharged slower with the available excess power. In this case, *bsfc* would be about 265g/kWh but the recharge time would increase.

In the ON-OFF strategy, the free power for maneuvers is limited. However, the charge of the battery could be interrupted if necessary and the powertrain could work in thermal mode.

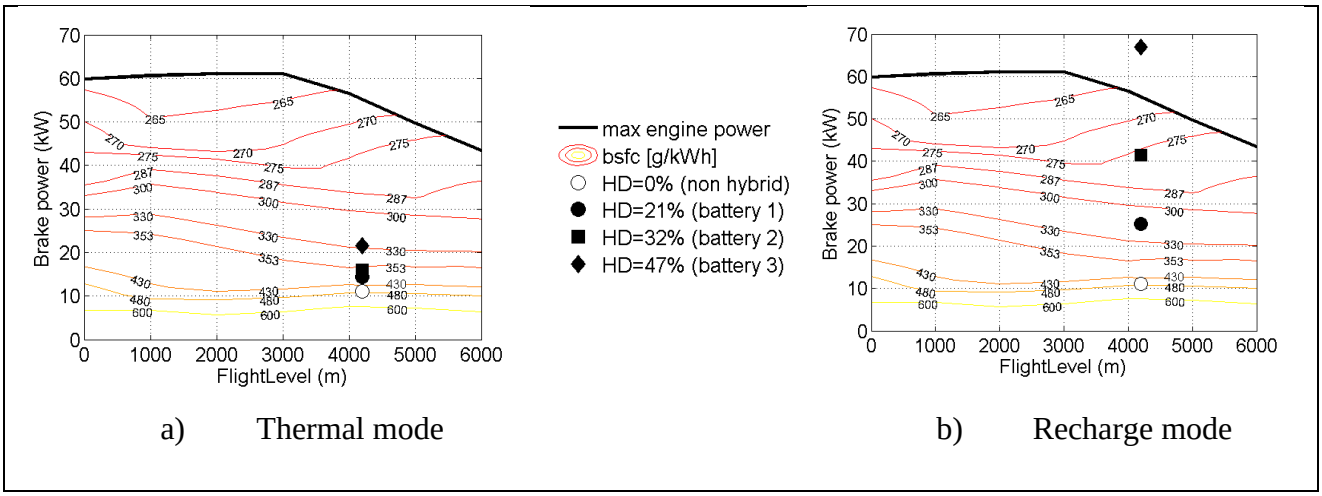

Figure 13 – Effect of battery specification on the engine working point

Figure 14 shows the specific endurance of the four powertrains with increasing HD and electric endurance. For each hybrid electric case, the thermal and ON-OFF strategies are compared. Note that Battery 3 cannot be recharged at I_0 in ON-OFF mode as already explained; therefore, this case is not reported in Figure 14.

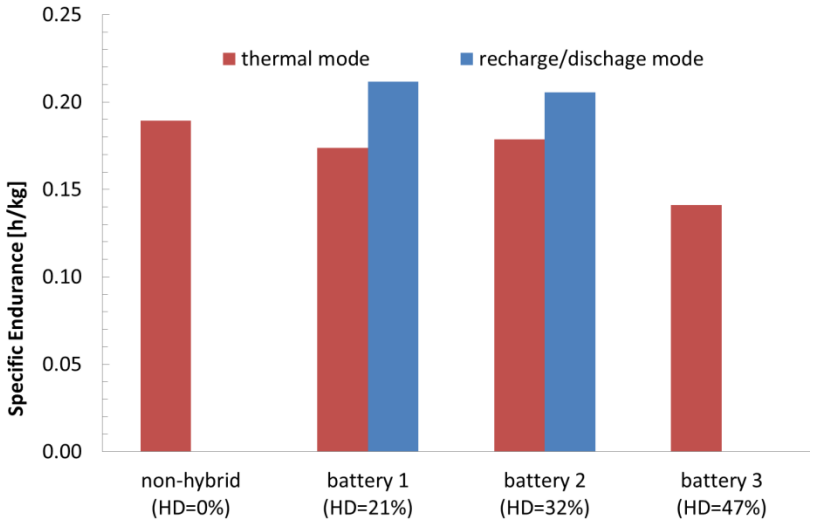

Figure 14 – Specific endurance of the hybrid electric power systems compared with a non-hybrid UAV

Note the trade-off between electric flight time and total endurance in the ON-OFF case. Battery 1 guarantees an electric flight time of 30 minutes and a specific endurance of 0.21h/kg, which is higher than baseline case by 12%. Battery 2 allows the UAV to fly in electric mode for 60 minutes with an improvement of specific endurance of 8% with respect to the non-hybrid case. In all cases, the ON-OFF strategy ensures better results than the continuous thermal operation mode that reaches the best specific endurance with the medium value of hybridization degree (32%).

Even if the proposed formula for endurance can be used to any parallel hybrid electric power systems with an ON-OFF energy management strategy, the results of Figure 14 cannot be generalized because they depend on the specific size and performance map of the engine. On the other hand, they are useful to stress the importance of optimizing the size of the components and the energy management strategy at the same time in a hybrid electric power system.

7 Conclusions

The present investigation proposes a formula to evaluate the endurance of a hybrid electric aircraft that fly at constant power with alternate cycles of charge and discharge (ON-OFF strategy).
The formula requires the calculation of the time, the power and the energy associated to the discharge and recharge processes of the batteries. A parallel hybrid electric power system with Lithium polymer batteries and two stroke diesel engines was considered. However, the methodology can be easily extended to other configurations and components of the powertrain.
Starting from a review of battery models available in literatures and using experimental data for lithium-polymer batteries, two amended discharge models were proposed. They allowed a reduction of the relative error from 22% to 3% with respect to the original ones. Both approaches require only generic information on the batteries that can be easily found in the manufacturer datasheet, like the nominal capacity and voltage, the depth of discharge and the burst discharge current. The time and energy needed to recharge the battery are also calculated with a pioneering method validated through experimental data.
In order to explain how these models can be applied to real applications, a parallel hybrid power system was sized and analyzed for a medium-altitude long-endurance unmanned aerial vehicle. The battery was sized to allow an electric flight time of 30, 60 and 90 minutes and three hybridization degree were taken into account as a consequence. A thermal mode and an ON-OFF strategy were considered for each hybrid power system and a conventional non hybrid case was used as reference. Therefore, a total of 7 cases were studied and the engine operating mode in each case was calculated with an altitude engine performance map. The takeoff mass of the aircraft increased from 500kg in the conventional case to about 900kg in the power system with the higher hybridization degree.
The effect of the battery sizing on the overall fuel economy was discussed together with the importance of accurately calculating the brake specific fuel consumption of the engine in the seven cases.

For the proposed test case, the ON-OFF strategy allowed a reduction of fuel consumption by 12% and 8% with respect to the non-hybrid case when the battery was sized for 30min and 60 min of electric flight, respectively. Even if the proposed formula for specific endurance can be used to any parallel hybrid electric power systems with an ON-OFF energy management strategy, the results of the test case cannot be generalized because they depend on the specific size and performance map of the engine. On the other hand, they are useful to stress the importance of optimizing the size of the components and the energy management strategy at the same time in a hybrid electric power system to better exploit the advantages of this technology.

8 Acknowledgments

The investigation has been funded by the Italian Ministry for Education, University and Research (project code PON03_00067_8) and is part of a research project of the Aerospace Technological District (DTA-Scarl). The authors would like to thanks prof. Traub and prof. Verstraete for kindly giving additional information about their experimental tests.

9 Nomenclature

bC_{rate}	Burst discharge current of the battery/C
BHP	Brake horse power
bsfc	Brake specific fuel consumption of the engine
C	nominal capacity
c_{D0}	Zero lift drag coefficient
C_{rate}	nominal discharge current of the battery/C
DOD	Depth of Discharge
E	Energy
EE	Electric Endurance
E_0, *J, H, P*	Parameters of the Sheperd-Peukert model
G	Flow rate
GED	Gravimetric energy density
h	Parameter of the proposed charge model
HD	Hybridization degree
I	current
I_0	Charging rate
K	Induced drag factor
k	Parameter of the proposed charge model. Final current of the battery charge=kI_0
L	percentage of the battery maximum power drawn from the battery
M	Mass
n	Peukert coefficient
Ns	Number of battery cells in series
OCV	Open Circuit Voltage
P	Power
R	Internal resistance of the battery
rC_{rate}	Maximum recharge current/C
S	Wing area
SE	Specific endurance
SOC	State of charge
t	time
THP	Thrust power
U	True air speed
V	voltage
W	Weight
η	Efficiency
ρ	Atmospheric air density

Subscripts

batt	Battery
burst	Burst
c	Conventional (non hybrid) power system
CC	Constant current
cell	Battery cell
CV	Constant voltage
d	Discharge
E	Empty
Eff	Pseudo-effective
f	Fuel
fin	Final
G	Electric machine in generator mode
h	Hybrid power system with the ON-OFF strategy
ICE	Internal combustion engine
in	Initial
inf	Lower bound value (ON-OFF strategy)
M	Electric machine in motor mode
max	Maximum value
min	Cutoff value
mR	Modified Ragone approach
mT	Modified Traub formula
nom	Nominal
P	Propeller
r	Recharge
R	Ragone approach
sl	Sea level
sup	Upper bound value (ON-OFF strategy)
t	Hybrid power system in thermal mode
T	Traub formula
to	Takeoff

10 References

1. Hepperle M. (2012), Electric Flight - Potential and Limitations. Energy Efficient Technologies and Concepts of Operation, 22-24 October 2012, Lisbon, Portugal.
2. McCormick B. W., (1995) *Aerodynamics, Aeronautics and Flight Mechanics*, John Wiley.
3. Traub L. W. (2011), Range and Endurance Estimates for Battery-Powered Aircraft, *Journal of Aircraft*, Vol. 48, No. 2.
4. Avanzini G., Giulietti F. (2013), Maximum Range for Battery-Powered Aircraft, Journal of Aircraft, 50, pp. 304-307.
5. Saw L. H., Ye Y., Tay, A. A. O., (2014), Electro-thermal analysis and integration issues of lithium ion battery for electric vehicles, *Applied Energy*, 131, 97-107.
6. Arista A., Ferraro M., Sergi F., Antonucci V. (2015) , Dynamic Model of High-Performance Li-ion cells (LiFePO4, Li-Polymers and LiFP6 NBC) in different load conditions, 6th IC-EpsMsO, Athene, ISSN: 2241-9209.

7. Traub L. W., (2013) Validation of endurance estimates for battery powered UAVs, *Aeronautical Journal*, Vol. 117, No. 1197.
8. Avanzini G., de Angelis E. L., Giulietti F. (2016), Optimal performance and sizing of a battery-powered aircraft, Aerospace Science and Technology, vol. 59, 132-144.
9. Donateo T., Ficarella A., Spedicato, L. , Arista A., Ferraro M. (2017) A new approach to calculating endurance in electric flight and comparing fuel cells and batteries, *Applied Energy*, Vol. 187, pp 807-819.
10. Fuller, M.E. (2014) A battery model for constant-power discharge including rate effects, *Energy Conversion and Management*, 88, 199–205.
11. Christen T., Carlen M. W. (2000), Theory of Ragone plots, *Journal of Power Sources* 91, 210-216.
12. Verstraete D., Gong ., Lu D. D.-C., Palmer J.L., (2015) Experimental investigation of the role of the batter in the AeroStack hybrid, fuel cell-based propulsion systems for small unmanned aircraft systems, *International Journal of Hydrogen Energy*, vol 40, pp 1598-1606.
13. Perullo C., Mavris D., (2014). A review of hybrid-electric energy management and its inclusion in vehicle sizing, *Aircraft Engineering and Aerospace Technology: An International Journal* 86/6 550-557.
14. Harmon F. H. (2006), Conceptual Design and Simulation of a Small Hybrid-Electric Unmanned Aerial Vehicle, Journal of Aircraft, Vol. 43, No. 5 1490-1498.
15. Merical K., Beechner T., Yelvington P. (2014), Hybrid-Electric, Heavy-Fuel Propulsion System for Small Unmanned Aircraft, SAE Technical paper, 2014-01-2222.
16. Oron H., (2006). UAV Engines in the next decade – Turbine Engines, Piston Engines and the newly Combat Proven Rotary Engine, A lecture at the 6th Symposium on Jet Engines and Gas Turbines, Haifa, Nov. 16, 2006.
17. Pornet C and Isikveren AT. (2015). Conceptual design of hybrid-electric transport aircraft, *Progress in Aerospace Sciences*, 79: 114-13.
18. Greiser C.M., Mengistu, I. H., Rotramel T. A., Harmon F.G., (2011). Testing of a Parallel Hybrid-Electric Propulsion System for use in Small Remotely-Piloted Aircraft", AIAA 2011-5903, 9th Annual International Energy Conversion Engineering Conference, 31 July – 3 August, San Diego, California.
19. Hung., J.K, Gonzalez L.F. (2012). On parallel hybrid-electric propulsion system for unmanned aerial vehicles, *Progress in Aerospace Science*, 51, pp 1-17.
20. Friedrich, C. and Robertson, P.A., (2014). Design of a hybrid-electric propulsion system for light aircraft, 14th AIAA Aviation Technology, Integration, and Operations Conference.
21. Cantore G., Mattarelli E., Rinaldini C.A. (2014). A new design concept for 2-Stroke aircraft Diesel engines, *Energy Procedia* 45, 739-748.
22. Nickol C. L., Guynn M. D., Kohour L.L., Ozorosku T. A. (2007). High Altitude Long Endurance Vehicle Analysis of Alternatives and Technology Requirements Development 45th AIAA Aerospace Sciences Meeting and Exhibit, 8-11 January 2007, Reno, Nevada.
23. Hendershot JR, Miller T. Design of Brushless Permanent-magnet Motors, 2nd ed. Lebanon, Ohio: Magna Physics Pub, 1994.

24. Snyder C. A., (2015). Exploring propulsion systems requirements for more and all-electric helicopters, International Symposium on Air Breathing Engines (ISABE); 22nd; 25-30 Oct. 2015; Phoenix, AZ; United States
25. Guzzella L., Sciarretta A., (2013), Vehicle Propulsion Systems: Introduction to modeling and optimization, 3rd edition, Springer.
26. Geng P, Wu W, Huang M, Blaabjerg F. (2013). Efficiency Analysis on a Two-level Three-Phase Quasi-Soft-Switching Inverter". In: Twenty-Eighth Annual IEEE Applied Power Electronics Conference and Exposition (APEC), Long Beach, CA, USA, 17 -21 March 2013.
27. www.lipolbattery.com [accessed 03.02.2017].
28. Brodd R. J., (2008), New High Energy/Power Devices, Workshop on Drug Discovery Approach to Breakthroughs in Batteries, September 8 and 9, 2008.
29. Baronti F., Fantechi G., Fanucci L, Leonardi E., Roncella R., Saletti R., Saponara S. (2011), State-of-charge Estimation Enhancing of Lithium batteries through a Temperature-Dependen Cell Model, 2011 International Conference on Applied Electronics (AE), 7-8 Sept. 2011.
30. Tremblay O., Dessaint L.-A, (2009), Experimental Validation of a Battery Dynamic Model for EV applications, World Electric Vehicle Journal Vol. 3, 2009.
31. Cai Y., Ouyang M.G., Yang F., (2017) Impact of power split configurations on fuel consumption and battery degradation in plug-in hybrid electric city buses, Applied Energy, Volume 188, Pages 257-269, ISSN 0306-2619
32. Li G., Zhang J., He H., (2017) Battery SOC constraint comparison for predictive energy management of plug-in hybrid electric bus, Applied Energy, Available online 6 October 2016, ISSN 0306-2619
33. Su Y., Liahng H., Wu J., (2008) Multilevel Peukert Equations Based Residual Capacity Estimation Method for Lead-Acid Batteries, IEEE International Conference on Sustainable Energy Technologies, IEEE Publ., Piscataway, NJ, pp. 101-105.
34. Ning G., Haran B., and Popov B. N. (2003), Capacity fade study of lithium-ion batteries cycled at high discharge rates, *Journal of Power Sources*, vol. 117, pp. 160–169.
35. Tremblay O., Dessaint L.-A., Dekkiche A.I., (2007) A Generic Battery Model for the Dynamic Simulation of Hybrid Electric Vehicles, IEEE Vehicle Power and Propulsion Conference 0-7803-9761-4/07.
36. Pregelj B., Micor M., Dolanc G., Petrovčič J., Jovan V., (2016) Impact of fuel cell and battery size to overall system performance – A diesel fuel-cell APU case study, *Applied Energy*, Volume 182, Pages 365-375, ISSN 0306-2619
37. Hausmann A., Depcik C. (2013), Expanding the Peukert equation for battery capacity modeling through inclusion of a temperature dependency, *Journal of Power Sources*, Volume 235, pp. 148-158.
38. Zhang C., Jiang J., Gao Y., Zhang W., Liu Q., Hu X., (2017) Charging optimization in lithium-ion batteries based on temperature rise and charge time, *Applied Energy*, Vol. 194, 569-577.
39. Battery and Energy Technologies, http://www.mpoweruk.com/lithiumS.htm#charging; [accessed 03.02.2017]

40. Lan-Rong D., Chieh-En C., Hsiang-Fu Y., (2016) A Robust, Intelligent CC-CV Fast Charger for Aging Lithium Batteries, IEEE 25th International Symposium on Industrial Electronics (ISIE), DOI: 10.1109/ISIE.2016.7744901.
41. Standalone Linear Li-Ion Battery Charger datasheet, http://cds.linear.com/docs/en/datasheet/405842fs.pdf [accessed 03.02.2017].
42. Rahimi-Eichi, Baronti F., Chow M-Y, (2014), Online Adaptive Parameter Identification and State-of-charge Coestimation for Lithium-Polymer Battery Cells, IEEE transactions on industrial electronics, Vool. 61, No. 4.
43. https://www.flitetest.com/ [accessed 03.02.2017].
44. Ng K. S., Moo C.-S., Chen Y.-P., Hsieh Y.-C., (2009). Enhanced Coulomb counting method for estimating state-of-charge and state-of-health of lithium-ion batterie, *Applied Energy*, 86, pp. 1506-1511.
45. Cousin M (2016), Electric Flight in Airbus Group: The E-Fan adventure and beyond, Electric and Hybrid Aerospace Symposium, Cologne, November 9-10, 2016.
46. Donateo, T., Spedicato, L., Trullo, G., Carlucci, A.P., Ficarella, A. (2015) Sizing and simulation of a piston-prop UAV Energy Procedia, 82, pp. 119-124
47. Bérubé D., Dessaint L. A., Liscouet-Hanke S., Lavoie C. (2011). Simulation of a hybrid emergency power system for more electric aircraft. Canadian Aeronautics and Space Journal, 57(3): 155-162, 10.5589/q11-018
48. Panagiotou P., Kaparos P. Salpingidou C., Yakinthos K. (2016) , Aerodynamic design of a Male UAV, Aerospace Science and Technology, 50, 127-138.
49. Olsen J., Page, J. R. (2014). Hybrid powertrain for light aircraft, *Int. J. Sustainable Aviation*, Vol 1-1.

Appendix

Complete formulas for current, voltage and power versus time during the CC-CV charge and for the corresponding charge time

$$I(t)=\begin{cases} I_0, & t\le t_{CC} \\ I_0 e^{\frac{-\log(\frac{1}{k})}{t_{CV}}(t-t_{CC})}, & t_{CC}<t\le t_{CC}+t_{CV} \end{cases}$$

$$V(t)=\begin{cases} N_s\left[m\cdot SOC(t)+q+RI_0\right]=mN_s\left(SOC_{in}+100\cdot\frac{I_0}{C}t\right)+qN_s+RI_0N_s, & t\le t_{CC} \\ mN_s\left(SOC_{in}+100\cdot\frac{I_0}{C}t_{CC}\right)+qN_s+RI_0N_s=V_{\max}N_s & t_{CC}<t\le t_{CC}+t_{CV} \end{cases}$$

$$P(t)=V(t)\cdot I(t)=\begin{cases} mN_sI_0\left(SOC_{in}+100\cdot\frac{I_0}{C}t\right)+qN_sI_0+RI_0{}^2N_s, & t\le t_{CC} \\ I_0V_{\max}N_se^{\frac{-\log(\frac{1}{k})}{t_{CV}}(t-t_{CC})} & t_{CC}<t\le t_{CC}+t_{CV} \end{cases}$$

Recharge energy is calculated as reported below:

$$E_{TOT}=\int_0^{u_{CC}}\left[mN_sI_0\left(SOC_{in}+\frac{1}{36}\cdot\frac{I_0}{C}u\right)+qN_sI_0+RI_0{}^2N_s\right]du+I_0V_{\max}N_s\int_{u_{CC}}^{u_{CC}+u_{CV}}e^{\frac{-\log(\frac{1}{k})}{u_{CV}}(u-u_{CC})}du=$$

$$N_s\left(mI_0SOC_{in}+qI_0+RI_0{}^2\right)\cdot u_{CC}+mN_s\frac{I_0{}^2}{72C}u_{CC}{}^2+I_0V_{\max}N_s\frac{1-k}{\log(\frac{1}{k})}u_{CV}=$$

$$N_s\left(mI_0SOC_{in}+qI_0+RI_0{}^2\right)\cdot u_{CC}+mN_s\frac{I_0{}^2}{72C}u_{CC}{}^2+36\cdot I_0V_{\max}N_s\left(SOC_{fin}-SOC_{in}\right)\cdot\frac{C}{I_0}-I_0V_{\max}N_su_{CC}=$$

$$N_s\left(mI_0SOC_{in}+qI_0+RI_0{}^2-I_0V_{\max}\right)\cdot u_{CC}+mN_s\frac{I_0{}^2}{72C}u_{CC}{}^2+36\cdot N_sI_0V_{\max}\left(SOC_{fin}-SOC_{in}\right)\cdot\frac{C}{I_0}=$$

$$36\cdot N_s\left(mI_0SOC_{in}+qI_0+RI_0{}^2-I_0V_{\max}\right)\cdot\left(SOC_{CC}-SOC_{in}\right)\frac{C}{I_0}+18\cdot mCN_s\left(SOC_{CC}-SOC_{in}\right)^2+$$

$$+36\cdot I_0V_{\max}N_s\left(SOC_{fin}-SOC_{in}\right)\cdot\frac{C}{I_0}$$

The model parameters *m* and *q* are calculated by considering a linear voltage increase in the constant current phase; u_{CC} is the time at which the constant current phase is completed and u_{CV} is the time needed for the constant voltage phase charging.